



Technical Memorandum 93-79

**Modelling Arctic Ambient Noise
in the 2 - 200 Hz band**

by

M.V.Greening and P.Zakarauskas

December 1993

UNLIMITED

DEFENCE RESEARCH ESTABLISHMENT PACIFIC

Research and Development Branch

Department of National Defence

Canada



DEFENCE RESEARCH ESTABLISHMENT PACIFIC

CFB Esquimalt, FMO Victoria, B.C. V0S 1B0

Technical Memorandum 93-79

Modelling Arctic Ambient Noise
in the 2 - 200 Hz band

UNLIMITED

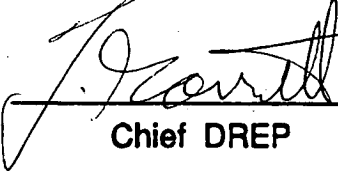
by

M.V. Greening and P. Zakarauskas

December 1993



Approved By:


Chief DREP

Research and Development Branch
Department of National Defence

Canada

Abstract

Short-term Arctic ambient noise spectra over the frequency band 2 - 200 Hz are presented along with a two-component noise model capable of reproducing these spectra. The model is based on the measured source spectrum and the spatial, temporal and source level distributions of both active pressure ridging and ice cracking. Modelled ambient noise levels are determined by summing the input energy of the distributions of ice cracking and pressure ridging events and correcting for the propagation loss. Both modelled and measured spectra show that ice cracking may dominate the spring-time ambient noise to frequencies as low as 40 Hz.

Résumé

Nous présentons des spectres de bruit arctique à court terme dans la bande de fréquences de 2 - 200 Hz ainsi qu'un modèle de bruit à deux composants capable de reproduire ces spectres. Le modèle est basé sur le spectre de la source mesurée ainsi que les distributions spatiale, temporaire et du niveau d'émission de la formation active de stries due à la pression aussi bien que de la fissuration des glaces. Nous déterminons les niveaux de bruit ambiant modélisés en totalisant l'énergie absorbée des distributions d'événements de fissuration des glaces et de formation de stries due à la pression et en faisant des corrections pour la perte de propagation. Les spectres modélisés aussi bien que les spectres mesurés montrent que la fissuration des glaces peut dominer le bruit ambiant au printemps jusqu'aux fréquences aussi basses que 40 Hz.

I Introduction

The long-term-averaged ambient noise spectrum of the Arctic Ocean over the frequency band of 1 - 1000 Hz exhibits two broad peaks centered near 15 Hz and 300 Hz (see Ref. 1). The peak near 15 Hz is believed to be due to active pressure ridging²⁻⁴ while the peak near 300 Hz has been shown to be caused by thermal ice cracking.⁵⁻⁷

Two important factors for many sonar applications are the short term variability of the ambient noise spectrum and the spatial distribution of sources which comprise the ambient noise. This paper examines the short term (2 min) fluctuations of Arctic pack ice ambient noise spectra over the frequency band 2 - 200 Hz and relates these fluctuations to environmental conditions. A two-component noise model is presented which incorporates both ice cracking and active pressure ridging, and is capable of reproducing the measured ambient noise spectra. This model shows the relative importance of each source term over the frequency band examined and was used to determine the maximum range which needs to be considered for each mechanism.

Ambient noise measurements are described in Sec. II while details of the two-component noise model are presented in Sec. III. A comparison between the model and measurements is shown in Sec. IV and a brief summary is given in Sec. V.

II Ambient Noise Measurements

The data analyzed in this paper were collected on the pack ice off the northern coast of Ellesmere Island over several days during April 1988. Details on the experimental setup and environmental conditions are available elsewhere.^{4,8-10}

A set of 69 two-minute samples of ambient noise was recorded with samples taken approximately every 1.5 hours over a 100-hour period. At the end of this data collection period, a pressure ridge became active approximately 2 km from the experimental site. Ambient noise measurements were recorded continuously for several hours during the time of this ridge building event.

The 69 two-minute samples of ambient noise were separated into four distinct classes by examining their power spectra (power levels are all given in dB relative to a source level of $1 \mu\text{Pa}^2/\text{Hz}$ at 1m). The four classes of spectra are shown in Figs. 1a - 1d. Class one (Fig. 1a) shows a peak with a level of approximately 86 dB at 8 Hz and a fall-off to 48 dB at 200 Hz. Class two (Fig. 1b) shows the same peak near 8 Hz but the fall-off at higher frequency has two stages, with a rapid decrease in level out to 35 Hz and a slower decrease beyond 35 Hz to a level of 57 dB at 200

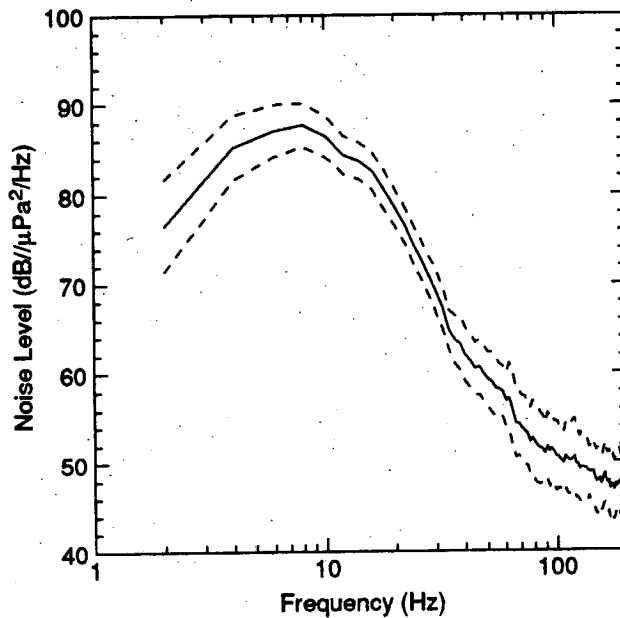


Figure 1: a). Average ambient noise spectra (solid) and standard deviation (dashed) for class 1 noise showing strong infrasonic peak at 8 Hz with little or no thermal ice cracking.

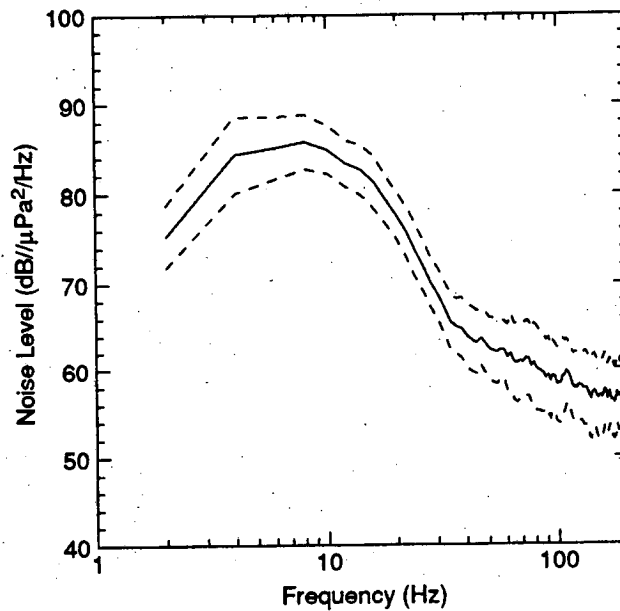


Figure 1: b). Average ambient noise spectra (solid) and standard deviation (dashed) for class 2 noise showing strong infrasonic peak at 8 Hz with some thermal ice cracking.

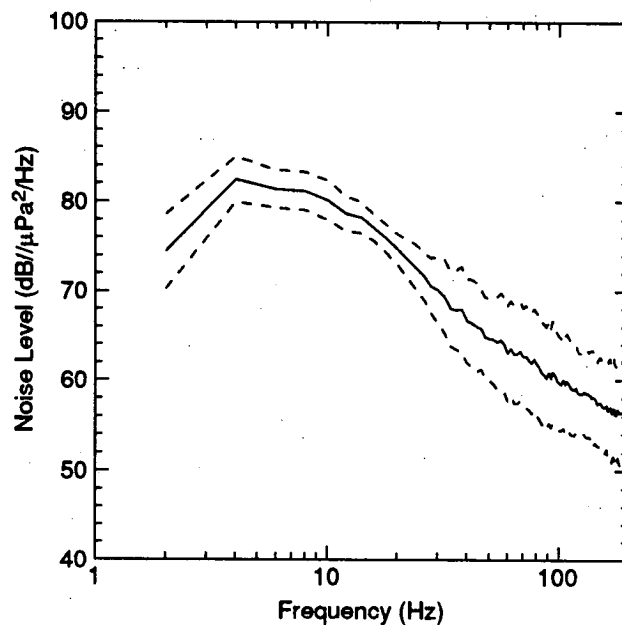


Figure 1: c). Average ambient noise spectra (solid) and standard deviation (dashed) for class 3 noise showing weaker and broader infrasonic peak at 4 Hz with some thermal ice cracking.

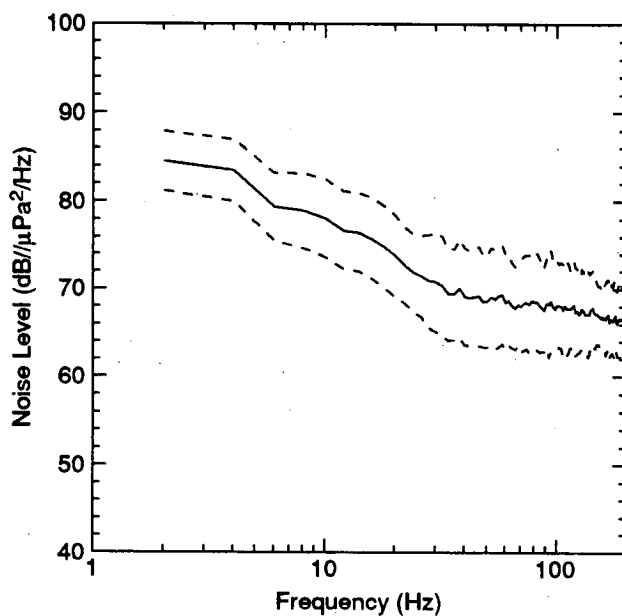


Figure 1: d). Average ambient noise spectra (solid) and standard deviation (dashed) for class 4 noise showing intense thermal ice cracking with no noticeable infrasonic peak.

Hz. Class three (Fig. 1c) shows a weaker and broader peak at 4 Hz with a fall-off at higher frequency to 58 dB at 200 Hz. Class four (Fig. 1d) shows a continuous but slow decrease in noise level with increasing frequency from a level of 85 dB at 2 Hz to 66 dB at 200 Hz. The minimum number of data sets used in any class was 14.

In Table I, the four classes of ambient noise spectra are correlated with environmental conditions and the number of detected ice cracking events occurring per minute. Details on the detection of individual ice cracking events are available in previous papers.^{8,10,11} The most striking feature of the comparison of ambient noise spectra with environmental parameters is the increase in noise levels above 35 Hz as both the temperature change becomes more negative and the number of detected ice cracking events per minute increases. This is consistent with previous measurements of thermal ice cracking and temperature change, although thermal ice cracking is usually associated with higher frequencies from 100 - 600 Hz (see Refs. 5-7, 12). It can also be seen that the noise levels above 35 Hz increase as the average solar radiation decreases and the solar radiation change becomes more negative; however, the large variance in these measurements makes any correlations suspect. The other noticeable feature of the comparison of ambient noise spectra with environmental parameters is the high wind speeds and barometric pressures associated with the strong peak at 8 Hz as seen in Figs. 1a and 1b. This agrees with previous measurements made by Makris and Dyer.¹³

The correlations between the ambient noise levels at 10 Hz and 200 Hz with the environmental conditions are shown in Table II. These show a very strong correlation between the ambient noise level at 200 Hz and both the number of detected events and a negative temperature change. A moderate correlation is also shown between the ambient noise level at 10 Hz and the barometric pressure. Again, this is consistent with the correlation study performed by Makris and Dyer.¹³ Surprisingly, the correlation between the noise level at 10 Hz and the wind speed was very low.

III Model

The goal of the two-component ambient noise model described below is to accurately model the ambient noise spectra observed in the Arctic pack ice over the frequency band 2 - 200 Hz. For these frequencies, the ambient noise is assumed to be produced mainly by ice cracking and active pressure ridging. Thus, by summing the acoustic field generated by the distribution of these events, the ambient noise can be reproduced and the relative contributions of each noise source at the receiver can be determined.

Table I: Mean and variance of measured environmental conditions and the number of detected ice-cracking events per minute for the four classes of measured power spectra shown in Figs. 1a - 1d. Temperature, barometric pressure and solar radiation changes were measured during a one-hour period prior to the ambient noise measurements.

Environmental Parameter	Class 1 Fig 1a	Class 2 Fig 1b	Class 3 Fig 1c	Class 4 Fig 1d
Current Speed (cm/sec)	3.0 ± 1.9	4.6 ± 1.8	4.5 ± 0.6	4.4 ± 1.3
Wind Speed (m/sec)	7.8 ± 1.5	7.2 ± 2.0	3.3 ± 2.0	4.6 ± 1.1
Temperature (°C)	-21.3 ± 1.4	-21.8 ± 2.3	-18.3 ± 2.1	-21.6 ± 2.3
Temp Change (°C/hour)	0.35 ± 0.16	-0.26 ± 0.16	-0.18 ± 0.15	-0.45 ± 0.30
Solar Radiation (W/m ²)	154 ± 70	123 ± 82	103 ± 73	65 ± 23
Solar Rad Change (W/m ² hour)	24 ± 34	-2 ± 30	5 ± 25	-18 ± 14
Barometric Pressure (in-Hg)	30.40 ± 0.07	30.35 ± 0.12	30.15 ± 0.11	30.22 ± 0.11
Bar Pres Change (in-Hg/hour)	0.00 ± 0.01	0.00 ± 0.01	0.01 ± 0.03	-0.02 ± 0.01
Detected Events (events/min)	1.0 ± 1.0	7.2 ± 5.6	3.3 ± 1.3	22.2 ± 5.2

Table II: Cross correlation between the measured ambient noise levels at 10 Hz and 200 Hz with the measured environmental conditions and the number of detected ice-cracking events per minute. Temperature, barometric pressure and solar radiation changes were measured during a one-hour period prior to the ambient noise measurements.

Environmental Parameter	Correlation Coefficient	
	10 Hz	200 Hz
Current Speed	-0.06	0.14
Wind Speed	0.18	-0.11
Temperature	-0.01	0.01
Temp Change	0.20	-0.72
Solar Radiation	0.28	-0.23
Solar Rad Change	0.20	-0.33
Barometric Pressure	0.52	-0.07
Bar Pres Change	-0.19	-0.05
Detected Events	-0.18	0.76

A. Pressure Ridging

Active pressure ridges occur when two ice sheets are pushed together, usually by wind or current, forcing one sheet over the other. This bends the sheets until the resulting stresses fracture the ice into large blocks which pile up forming long rows with a cone shaped vertical cross section. We showed in a previous paper⁴ how the source spectrum level of an active pressure ridge, when corrected for the propagation loss of a distant event at 60 km or more, produces the infrasonic peak found in the Arctic ambient noise spectra. The full effects of pressure ridging on the ambient noise spectra from 2 - 200 Hz will be examined here. Also the effects on the ambient noise of changing the bottom or ice interaction components of the propagation loss will be examined.

A simple method of determining the role of active pressure ridges on the ambient noise would be to sum the received energy from all occurring active ridges at a given time. However, this requires knowledge of the spatial, temporal and source level distributions of pressure ridges that are active when measurements are made; none of these is known at the present.

Sonar measurements of the under surface of the ice made by the USS Nautilus¹⁴ give an average of 6 keels/km across the entire Arctic basin. Laser altimetry measurements of the upper surface of the ice show reasonable agreement, with an average

ridge separation of approximately 100 m (see Ref. 15). However, these measurements show the sum of both active and old, inactive ridges. Members of the Defence Research Establishment Pacific have been conducting experiments in the Arctic pack ice over spans of one or more months each year since 1986 and the occurrence of an active pressure ridge at or near an experimental site is very rare. This suggests that active pressure ridges are only a small fraction of the ridges observed using sonar or laser altimetry. Buck and Wilson³ estimate an average active pressure ridge separation of 37 km to account for the ambient noise levels and compare this to pan sizes of 10 - 100 km measured by SEASAT SAR. (Pans are defined as groups of ice floes which move together.) Because of the large spatial separation of active pressure ridges, the component of ambient noise caused by pressure ridging may be dominated by a single or a small number of events occurring at some large distances from the array. Thus, examining a single pressure ridging event as a function of range may provide insight into the role of pressure ridging on the ambient noise. This requires only knowledge of the source spectrum level and the propagation loss.

The received spectrum of an active pressure ridge at approximately 2 km range is shown in Fig. 2. More details on this event are available in another paper.⁴ The source spectral level estimated from this received level is found to be monotonously decreasing and agrees with the source level per unit length of an active pressure ridging event measured by Buck and Wilson.³ The spectral shape we observed persisted for at least 1.5 hours with a continuous rise in level of approximately 15 dB over the first thirty minutes followed by a relatively consistent ambient noise level over the next sixty minutes with the exception of two or three large pulses occurring every minute with durations of five to tens of seconds and levels 10 - 15 dB above the ambient level. The absolute levels shown in Fig. 2 correspond to one of the pulses observed after the initial thirty minute rise. The pressure ridge remained active for approximately 6 hours while the event recorded by Buck and Wilson lasted approximately two days.³

When the spectrum level of pressure ridging shown in Fig. 2 is corrected for propagation loss, the resulting spectrum of a very distant ridging event exhibits a broad peak at 10 - 30 Hz as shown in Fig. 3. This peak resembles the infrasonic peak found in many real ambient noise spectra with the exception that the modelled ambient noise level remains relatively flat until 30 - 60 Hz while the real ambient noise level often begins decreasing at 10 - 20 Hz (Figs. 1a, 1b). The modelled results also show that the peak narrows as the range of the event increases. This suggests that the infrasonic peak could be explained if active pressure ridges were separated by several hundred kilometers. However, this disagrees with measurements of pan sizes so we must look at the propagation model to find an alternative explanation for the narrow peak.

The propagation loss was modelled using SAFARI¹⁶ (Seismo-Acoustic Fast field Algorithm for Range Independent environments) for the environmental conditions given in Table III. A flat bottom was used in the modelling and this was confirmed by a seismic survey which showed the bottom to be acoustically flat to beyond 1000

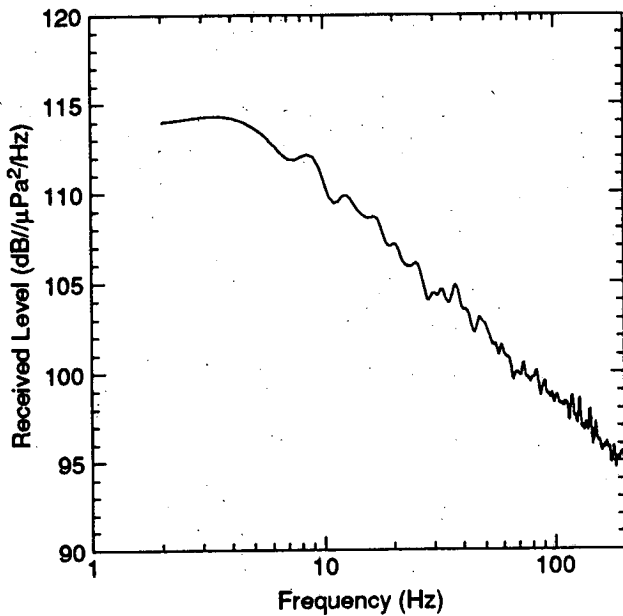


Figure 2: *Received source spectrum level of ridge building event at 2 km range.*

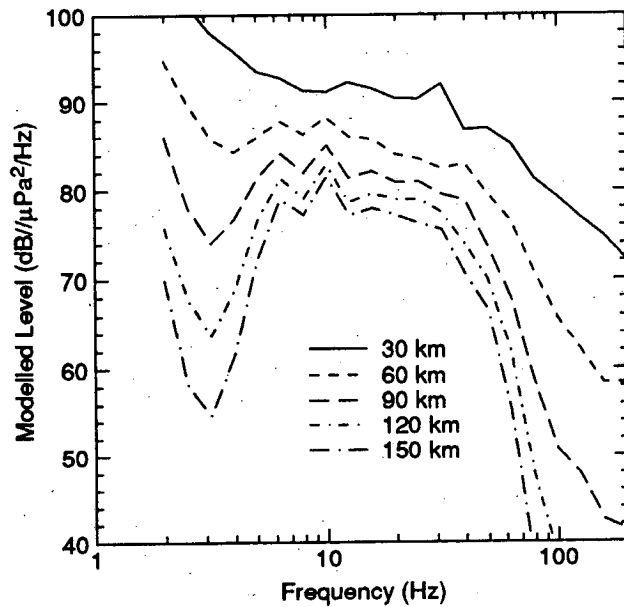


Figure 3: *Resulting ambient noise spectra produced by distant ridge building events using the environmental conditions given in Table III to determine propagation loss.*

Hz and by depth measurements within a few kilometers around the array which indicated a shallow slope of less than 1° . Measurements of the ice roughness were not obtained during the experiment but are based on typical sonar measurements from submarines¹⁷ and observations of the ratio of keel depth to sail height.¹⁵ The propagation model, SAFARI, considers the elastic properties of the ice and bottom layers along with scattering of a compressional wave in the water into both compressional and vertically-polarized shear waves in the ice and bottom. However, this model uses the Kirchhoff approximation of small roughness with small slope to estimate interface roughness. Both measurements¹⁵ and modelling¹⁸ show that ridge keels form in a roughly elliptical shape with keel depths as large as 10 times the ice thickness and ridge widths often as small as 3 times the keel depth. Thus, the Kirchhoff approximation is a very poor estimate of the under-ice roughness, especially at the shallow grazing angles involved with long range propagation, and will lead to an underestimation of the propagation loss. Livingston and Diachok¹⁹ used matched field processing to estimate the under-ice reflectivity at 18 Hz and 24 Hz along several tracks. They found the scattering loss to be approximately 10 times as large as that predicted using SAFARI.

Table III: Parameters of ice and bottom layers used for propagation loss modelling in SAFARI. C_p and C_s are the sound speeds for the compressional and shear waves while K_p and K_s and the compressional and shear wave attenuations.

	Ice	Bottom	Sub-Bottom
Thickness (m)	6	15	-
Density (g/cm ³)	0.9	1.8	1.9
C_p (m/sec)	2800	1800	2000
C_s (m/sec)	1750	300	500
K_p (dB/ λ)	2.0	0.5	0.5
K_s (dB/ λ)	3.0	0.25	0.25
RMS roughness (m)			
upper	1.0	-	-
lower	4.0	-	-

A scattering model using elliptically striated surfaces as a close approximation to ridge keels was first developed by Burke and Twersky.²⁰ This model considers the high angle slopes of ridge keels but is an inelastic model and thus also results in an underestimation of the propagation loss. Also, this model depends on the fourth power of ridge dimensions, which introduces large uncertainties. Finally, this model works by estimating the under-ice reflection coefficients but does not actually include an ice layer. Thus, it may be suitable when both the source and receivers are in the water column but will not include the effects of a source in the ice.

In an effort to reproduce the propagation loss caused by under-ice scattering, the absorption loss in the ice was allowed to increase. Although this is an entirely different loss mechanism, it has the desired characteristics of increasing the loss with increasing frequency and with each interaction with the ice. The resulting spectrum of a ridging event 90 km away for varying ice absorptions is shown in Fig. 4. This clearly shows that as the ice absorption increases, the modelled infrasonic peak narrows and becomes a better approximation of the peak observed in the real data in Figs. 1a and 1b.

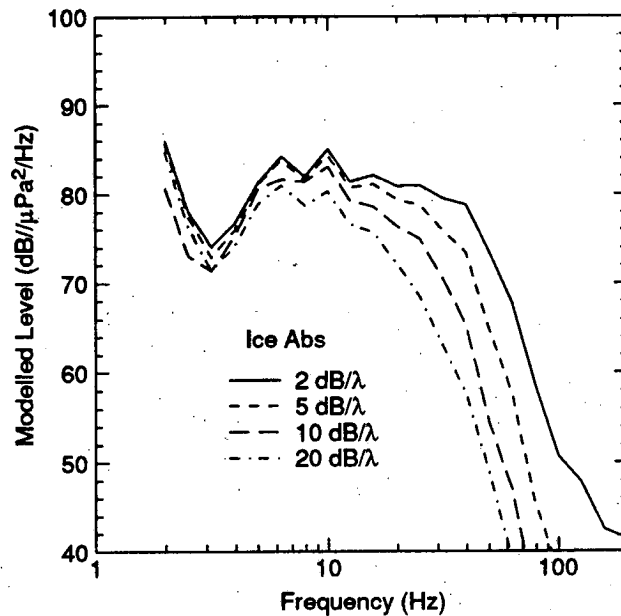


Figure 4: Resulting ambient noise spectra produced by a ridge building event at 90 km range for different levels of ice absorption. Levels of absorption for the compressional wave in the ice are given in dB/λ with shear wave absorption 1.5 times the compressional wave absorption.

Finally, because of the uncertainty in bottom shear characteristics, the effects of small changes in the shear wave speed and absorptions in the bottom layers were examined. These are shown in Figs. 5a and 5b. These figures use the environmental conditions given in Table III with the exception that the absorption in the ice is five times higher to compensate for the effects of under-ice roughness. Fig. 5a shows that as the bottom shear wave speed increases, the infrasonic peak in the ambient noise spectrum becomes more pronounced and shifts slightly towards higher frequency. Fig. 5b shows that the infrasonic peak also becomes more pronounced as the shear wave absorption increases.

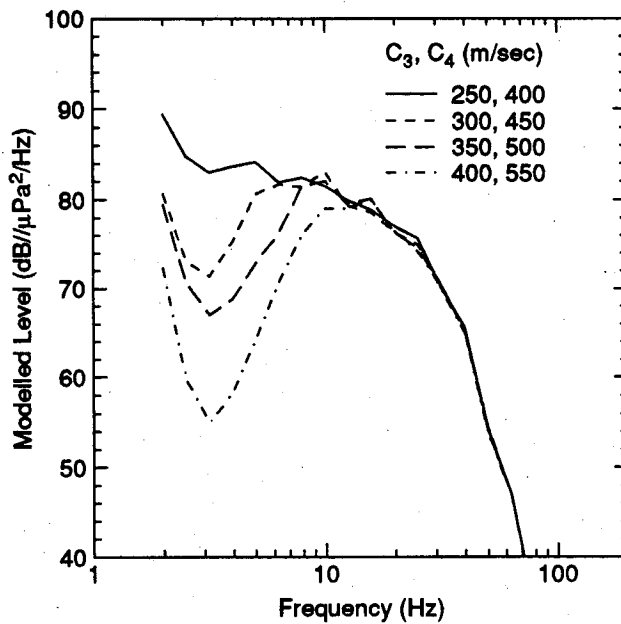


Figure 5: a). Resulting ambient noise spectra produced by a ridge building event at 90 km range for different bottom shear wave speeds. Speeds are given in m/sec for bottom (C_3) and sub-bottom (C_4) layers.

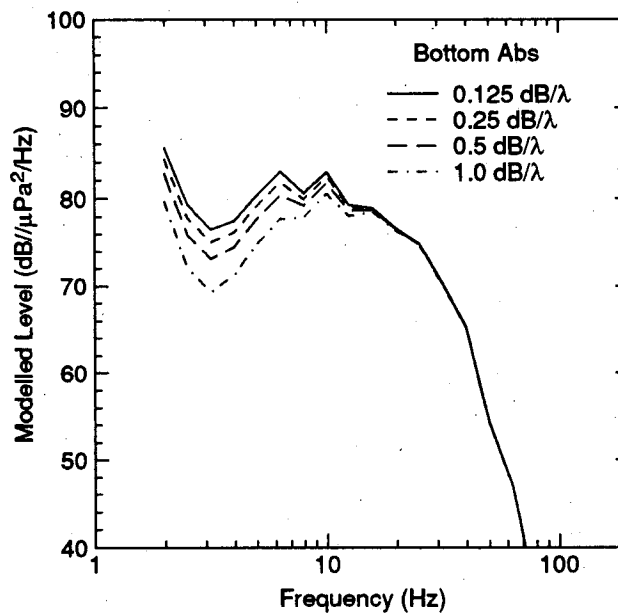


Figure 5: b). Resulting ambient noise spectra produced by a ridge building event at 90 km range for different bottom shear wave absorptions. Both bottom layers use the same level of absorption given in dB/λ.

B. Thermal Ice Cracking

Thermal ice cracks are small ice fracturing events which occur near the surface of the ice as it contracts during times of atmospheric cooling. By using the spatial, temporal and source level distributions of thermal ice cracking, the average energy per unit area entering the water due to thermal ice cracking can be determined. This in turn is used to determine the average energy received at a hydrophone suspended below the ice by integrating the energy input over all locations about the hydrophone and subtracting the associated propagation loss for each location.

In order to develop the thermal ice cracking component of the ambient noise model, the spatial, temporal and source level distributions along with the source spectrum and directivity of thermal ice cracking must be known. These have been measured and reported in previous papers^{8,10} and will be briefly outlined here.

The spatial distribution of events over the entire set of 69 two-minute samples was found to be uniform. This gives some justification to the proposed model of determining an average input energy per unit area. Note however that two forms of short-term fluctuations of the average input energy can occur. The first is a strength fluctuation in the overall input level applied to all locations as the rate of ice cracking changes. The second is a random statistical fluctuation in the spatial distribution which may cause local areas of weak or intense ice cracking. These random statistical fluctuations have more effect on the ambient noise when occurring at close range due to the smaller number of events and lower propagation loss associated with close range. Thus, statistical fluctuations will be applied only within 1 km of the hydrophone. These two types of fluctuations could account for some of the differences between classes of real ambient noise spectra noted in the previous section and are included in the model.

For the 2 - 200 Hz frequency band observed, the source directivity of thermal ice cracking was found to be well described by a monopole in the ice⁸ while the source spectrum was found to be relatively flat.¹⁰ Thus, the source strength distribution of these events does not depend on frequency for this frequency band. Source levels of detected events were measured in the range of 110 - 180 dB// $\mu\text{Pa}^2/\text{Hz}$ at 1m, with the median temporal and source level distribution as shown in Fig. 6. This distribution approximates a linearly decreasing function on a log-dB scale of the number of events versus source level. The decrease in the number of events with increasing source level is proportional to $10^{-\alpha SL}$ with $\alpha \approx 0.08$ for source levels below 160 dB// $\mu\text{Pa}^2/\text{Hz}$ at 1m, and $\alpha \approx 0.12$ for source levels above. (The shape of the source level distribution curve of Fig. 6 is similar to the measured distribution of earthquake magnitudes reported by Gutenberg and Richter.²¹) The mean of the source level distribution was found to be twice the median. A mean of 8 events/km²min occur over a 1 dB band of source levels centered at 110 dB// $\mu\text{Pa}^2/\text{Hz}$ at 1m.

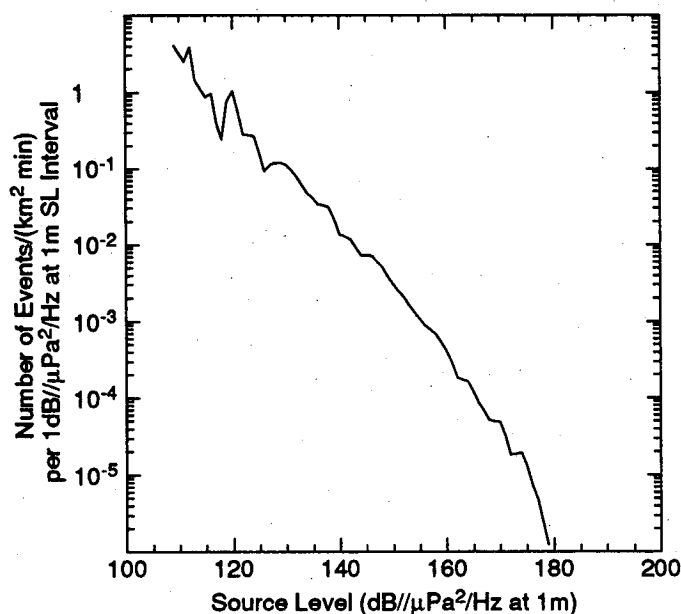


Figure 6: Median number of thermal ice cracking events per square kilometer per minute per 1 dB// μPa^2 /Hz at 1m source level interval versus source level.

Using the temporal and source level distributions given in Fig. 6 along with the fact that the events are spatially uniform, the mean energy input into the ice per square kilometer as a function of source power can be determined as:

$$E(P) = \delta t N(P) P$$

where $N(P)$ is the mean number of events occurring at source power P per square kilometer per minute, and δt is the mean time duration of an event in minutes. From our data, δt was found to be approximately 0.0017 minutes (0.1 seconds). The total average energy entering the ice per square kilometer is then obtained by summing over all source powers as:

$$E = \delta t \sum_{P=P_{min}}^{P_{max}} N(P) P.$$

When summing over only the observed source powers ($P_{min} = 0.1 \text{ Pa}^2$, $P_{max} = 10^6 \text{ Pa}^2$), the average energy input is 116.6 dB/km²// μPa /Hz at 1m. When extended 50 dB above and below the observed powers (from $10^{-6} - 10^{11} \text{ Pa}^2$) using the $10^{-\alpha SL}$ fit ($SL = 10 \text{ Log } P$ with P given in μPa^2), the average energy input increased by only 1.1 dB. Because the true minimum and maximum source powers are unknown,

the average energy input of $116.6 \text{ dB/km}^2/\mu\text{Pa}^2/\text{Hz}$ at 1m is used and the small increase obtained by extending the range of source powers will be ignored.

Using the average energy input per square kilometer calculated above, the average energy received at a hydrophone from a given source location is simply the average input minus the propagation loss associated with that location. The average received energy is then summed over all possible source locations to determine the ambient noise produced by thermal ice cracking. Our model steps out in range increments of 100 m to a total range of 200 km and determines the input energy for each range increment based on the area of the annulus $\pi(r_{max}^2 - r_{min}^2)$. Propagation loss is then averaged from the midrange of the annulus to 21 equispaced receivers from 100 - 300 m depth using the SAFARI propagation model. An arbitrary maximum range of 200 km was chosen based on the propagation model used but later results show that much shorter maximum ranges could have been used.

Finally, the short term fluctuations in the strength distribution and the random statistical fluctuations in the spatial distribution of thermal ice cracking must be modelled. The strength distribution of Fig. 6 represents an average distribution over the entire observation period. Insufficient data exists to produce separate distributions for intense or quiet times of ice cracking and these times are assumed to result in a strength distribution curve which is simply shifted up or down respectively. This shift can be estimated for real data by comparing the number of events detected per minute for a data sample with the average number of events detected per minute for all the data used to produce the strength distribution curve. For all 69 data files used in the strength distribution curve, the average number of detected events per minute was 6.6. Thus, for Fig. 1d, with an average of 22.2 events detected per minute, the strength distribution curve is assumed to be shifted up by a factor of 3.4. This in turn results in an increase in the average input energy per square kilometer by a factor of $10 \text{ Log}(3.4) = 5.3\text{dB}$.

The random statistical fluctuations in the spatial distribution have a large effect on the ambient noise levels when occurring at small range. This effect is included by varying the average input noise level within 1 km of the hydrophone. Ignoring short term strength fluctuations, the modelled ambient noise due to thermal ice cracking is shown in Fig. 7 for the input noise level within 1 km of the array varying from -20 to +20 dB relative to the average input noise level. When short term strength fluctuations are included, the curves in Fig. 7 are simply shifted up or down by the appropriate factor. Thus, to model the real data in Fig. 1d, the curves of Fig. 7 are shifted up by 5.3 dB as determined in the previous paragraph. Ice and bottom characteristics used to produce Fig. 7 are given in Table III with the exception that compressional and shear wave absorptions in the ice were five times higher in an attempt to better compensate for the effects of under-ice roughness. (Higher ice absorption was also required to accurately model received levels from active pressure ridges as shown in the previous section.) For frequencies above 40 Hz, Fig. 7 shows the general characteristics of the real data shown in Figs. 1a - 1d.

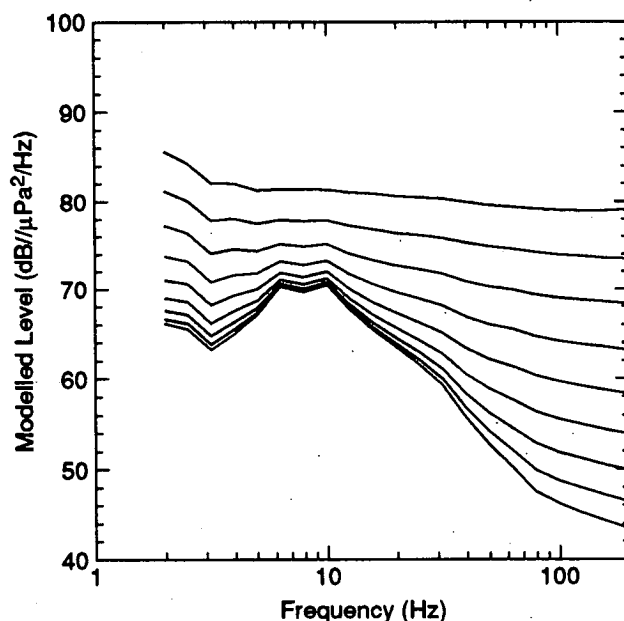


Figure 7: *Modelled thermal ice cracking noise. The close range input noise (within 1 km of the array) varies from -20 dB (lower curve) to +20 dB (upper curve) relative to the average input noise level with a 5 dB interval between individual curves.*

A comparison between real and modelled data above 40 Hz shows the validity of allowing the close range input noise to vary. Fig. 1a, which is approximated by a close range input noise level that is lower than average, represents data files with very few detected thermal ice cracking events. Of those events detected, only two events were within 1 km of the array and the received level of both these events was less than the ambient noise level at the time (events with a negative SNR can still be detected because of the array gain of the vertical array). At the other extreme, Fig. 1d, which is approximated by a higher-than-average close range input noise level, represents data files with many detected thermal ice cracking events. These data files were each found to contain several events within 1 km of the array with received levels at least 15 dB higher than the background ambient noise level. No other data files contained such events.

Finally, the thermal ice cracking model outlined above is capable of determining the relative contribution of close versus far range events in producing the ambient noise. Fig. 8 shows the required range to model 80% (within 1 dB) of the total noise energy produced from all thermal ice cracking events out to a range of 200 km. This is independent of the short term strength fluctuations but does depend on the short term spatial fluctuations. For frequencies near 10 Hz, if the local (within 1 km) thermal ice cracking level is low, events beyond 100 km must be considered to model the thermal ice cracking noise. However at this frequency, unless local thermal ice cracking levels are high, the ambient noise is dominated by pressure ridging and

thermal ice cracking need not be considered. For frequencies above 40 Hz, events within 30 km range suffice to model the total ambient noise to within 1 dB.

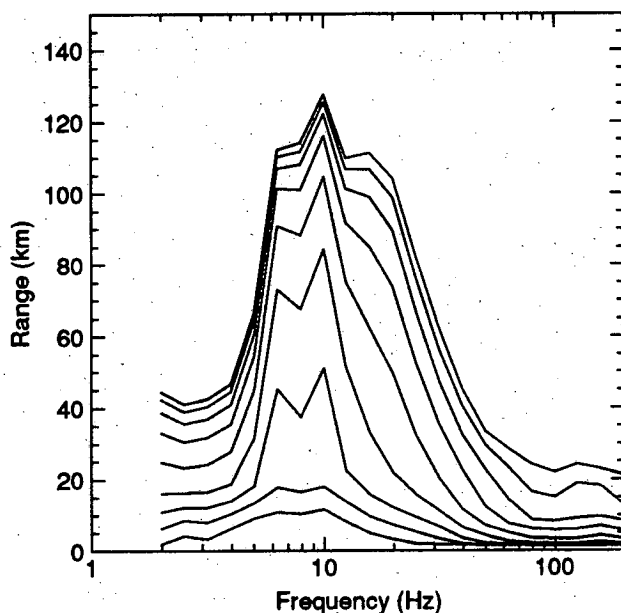


Figure 8: Required range to model 80% (within 1 dB) of the total noise produced from all thermal ice cracking events out to a range of 200 km. Close range input noise (within 1 km) varied from -20 dB (upper curve) to +20 dB (lower curve) relative to the average input noise level with a 5 dB interval between individual curves.

IV Results

A comparison of the two-component noise model with the four classes of measured real ambient noise spectra is shown in Figs. 9a - 9d. The measured and estimated bottom and ice parameters from Table III were used to determine propagation loss for the model with the exception that the compressional and shear wave absorptions used in the ice were five times higher (10.0 and 15.0 dB/ λ respectively) in an effort to better compensate for the effects of under-ice roughness. These figures show that the measured ambient noise spectra can be reproduced by a single active pressure ridging event, along with a distribution of thermal ice cracking events. For frequencies below 40 Hz, the ambient noise spectrum may be determined by the range and level of the strongest received active pressure ridge. For frequencies above 40 Hz, the ambient noise spectrum is determined by thermal ice cracking, with overall levels and spectral shape dependent on the intensity of ice cracking and the strength of local events relative to the average. For purposes of our model, local events are considered to be within 1 km of the hydrophone.

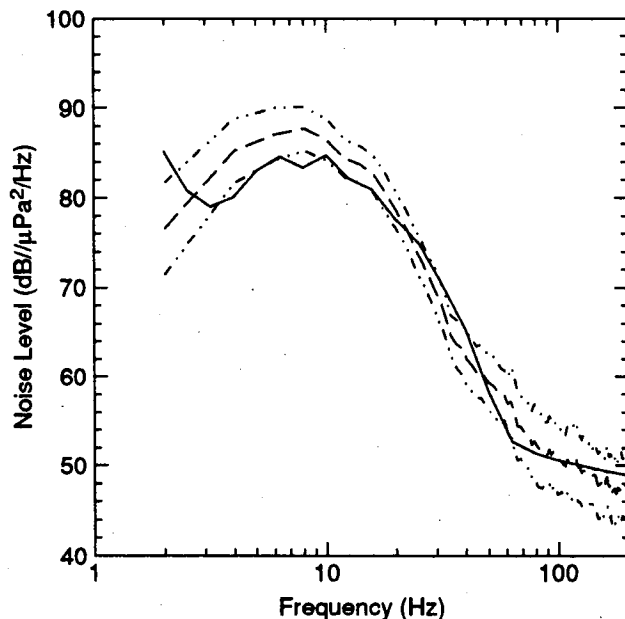


Figure 9: a). Comparison of two-component noise model (solid) with the average ambient noise (dash) and standard deviation (dash-dot) of class 1 real noise from Fig. 1a. Modelled noise contains a ridge at 70 km range with a source level +3 dB relative to that shown in Fig. 2, thermal ice cracking of -8.2 dB relative to average input energy determined from Fig. 6, and local ice cracking at -3 dB.

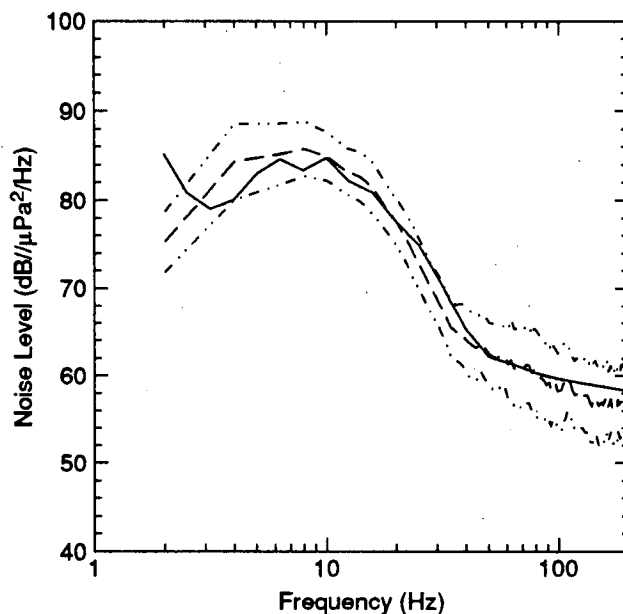


Figure 9: b). Comparison of two-component noise model (solid) with the average ambient noise (dash) and standard deviation (dash-dot) of class 2 real noise from Fig. 1b. Modelled noise contains a ridge at 70 km range with a source level +3 dB relative to that shown in Fig. 2, thermal ice cracking of +0.4 dB relative to average input energy determined from Fig. 6, and local ice cracking at +0 dB.

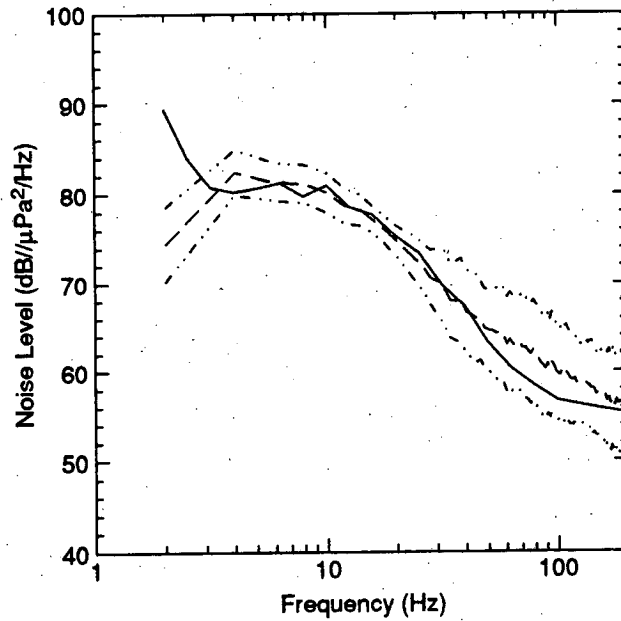


Figure 9: c). Comparison of two-component noise model (solid) with the average ambient noise (dash) and standard deviation (dash-dot) of class 3 real noise from Fig. 1c. Modelled noise contains a ridge at 40 km range with a source level -5 dB relative to that shown in Fig. 2, thermal ice cracking of -3.0 dB relative to average input energy determined from Fig. 6, and local ice cracking at +0 dB.

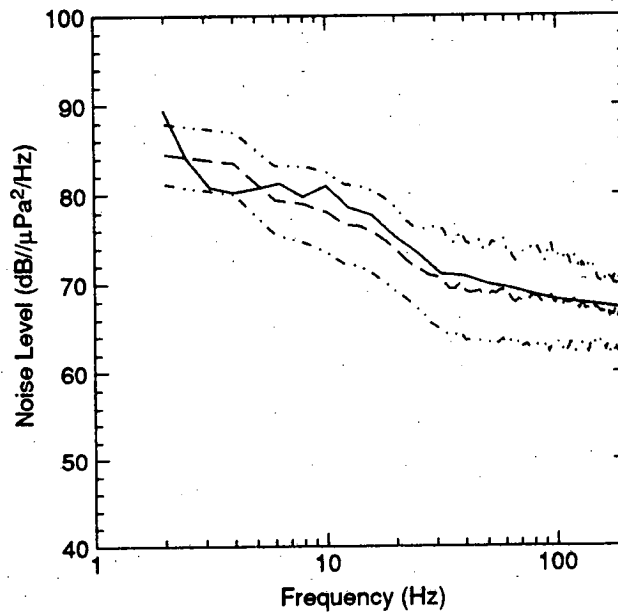


Figure 9: d). Comparison of two-component noise model (solid) with the average ambient noise (dash) and standard deviation (dash-dot) of class 4 real noise from Fig. 1d. Modelled noise contains a ridge at 40 km range with a source level -5 dB relative to that shown in Fig. 2, thermal ice cracking of +5.3 dB relative to average input energy determined from Fig. 6, and local ice cracking at +4 dB.

It was also noted that all of the data files used in classes 1 and 2 for real data occurred during a 66 hour span within the middle of the experiment while all except one of the data files used in classes 3 and 4 occurred before or after this time. This suggests that active pressure ridging was occurring at approximately 40 km range during the entire 100 hours of ambient noise measurements and that for a 66 hour span of time in the middle of the experiment, a much stronger pressure ridge was active at a range of approximately 70 km. Although the stronger and more distant active pressure ridge appears to be associated with times of weaker thermal ice cracking, no correlation is assumed due to the short time sample and the fact that the two source mechanisms are controlled by different environmental conditions.

Finally, it can be noticed from Figs. 9a - 9c that the modelled ambient noise spectra have negative slope below 3 Hz while the measured spectra have a positive slope. The reason for this discrepancy is unknown but may be due to the assumed spectral shape of active pressure ridging which was based on measurements from a single event using equipment which was not very reliable below 4 Hz.

V Summary

We have shown that the spring-time Arctic ambient noise spectrum measured in the pack-ice over the frequency band 3 - 200 Hz can be modelled by a combination of active pressure ridging and thermal ice cracking. A single or few active pressure ridges at ranges of tens of kilometers produces the low frequency end of the ambient noise spectrum up to approximately 40 Hz, while a distribution of thermal ice cracking events produces the higher end. Over 80% of the ambient noise produced by thermal ice cracking is generated by events occurring within 30 km of the hydrophone.

References

1. I.Dyer, "The song of sea ice and other Arctic Ocean melodies", in *Arctic Technology and Policy*, eds: I.Dyer and C.Chryssostomidis, McGraw-Hill, New York, 1984.
2. R.S.Pritchard, "Arctic Ocean background noise caused by ridging of sea ice," *J.Acoust.Soc.Am.*, **75**, 419-427 (1984).
3. B.M.Buck and J.H.Wilson, "Nearfield noise measurements from an Arctic pressure ridge," *J.Acoust.Soc.Am.*, **80**, 256-264 (1986).
4. M.V.Greening and P.Zakarauskas, "Pressure ridging source spectrum level and a proposed origin of the infrasonic peak in Arctic ambient noise spectra," accepted to be published in *J.Acoust.Soc.Am.*
5. A.R.Milne and J.H.Ganton, "Ambient noise under Arctic sea ice," *J.Acoust.Soc.Am.*, **36**, 855-863 (1964).
6. J.H.Ganton and A.R.Milne, "Temperature and wind-dependent ambient noise under midwinter pack ice," *J.Acoust.Soc.Am.*, **38**, 406-411 (1965).
7. A.R.Milne, "Thermal tension cracking in sea ice: A source of underice noise," *J.Geophys.Res.*, **77**, 2177-2192 (1972).
8. M.V.Greening, P.Zakarauskas and R.I.Verrall, "Vertical directivity of ice cracking," *J.Acoust.Soc.Am.*, **92**, 1022-1030 (1992).
9. P.Zakarauskas, R.I.Verrall and M.V.Greening, "Extraction of the seabed reflectivity function using ice cracking noise as a signal source," to be published in *J.Acoust.Soc.Am.* (Dec, 1993).
10. M.V.Greening and P.Zakarauskas, "Spatial and source level distributions of ice cracking in the Arctic Ocean," accepted to be published in *J.Acoust.Soc.Am.*
11. P.Zakarauskas, C.J.Parfitt and J.M.Thorleifson, "Automatic extraction of spring-time Arctic ambient noise transients," *J.Acoust.Soc.Am.*, **90**, 470-474 (1991).
12. Y.Xie and D.M.Farmer, "Acoustical radiation from thermally stressed sea ice," *J.Acoust.Soc.Am.*, **89**, 2215-2231 (1991).
13. N.C.Makris and I.Dyer, "Environmental correlates of pack ice noise," *J.Acoust.Soc.Am.*, **79**, 1434-1440 (1986).
14. A.S.McLaren, "Analysis of the under-ice topography in the Arctic Basin as recorded by the USS Nautilus during August 1958," *J. Arctic Institute of North America*, **41**, 117-126 (1988).
15. O.I.Diachok, "Effects of sea-ice ridges on sound propagation in the Arctic Ocean," *J.Acoust.Soc.Am.*, **59**, 1110-1120 (1976).

16. H.Schmidt, "SAFARI, Seismo-Acoustic Fast field Algorithm for Range Independent environments, User's guide," Rep. SR-113, SACLANT Undersea Research Center, San Bartolomeo, Italy, 1988.
17. L.A.LeShack, "Arctic Ocean deformation chart using sonar data recorded from nuclear submarines," Seventh Intl. Conf. on Port and Ocean Engineering under Arctic Conditions, Vol 1, 148-157, 1983.
18. R.R.Parmerter and M.D.Coon, "Model of pressure ridge formation in sea ice," J.Geophys.Res., 77, 6565-6575 (1972).
19. E.Livingston and O.Diachok, "Estimation of average under-ice reflection amplitudes and phases using matched-field processing," J.Acoust.Soc.Am., 86, 1909-1919 (1989).
20. J.E.Burke and V.Twersky, "Scattering and reflection by elliptically striated surfaces," J.Acoust.Soc.Am., 40, 883-895 (1966).
21. B.Gutenberg and C.F.Richter, *Seismicity of the earth and associated phenomena*, Princeton University Press, Princeton, New Jersey, 1954.

DREP TECHNICAL MEMORANDUM 93-79

Dist. List.

SECURITY GRADING: UNCLASSIFIED

3 - DSIS
Circulate to:
DRDM
DIUP

1 - DREA

6 - DREP

DOCUMENT CONTROL DATA

(Security classification of title, body of abstract and indexing annotation must be entered when the overall document is classified)

1. ORIGINATOR (the name and address of the organization preparing the document. Organizations for whom the document was prepared, e.g. Establishment sponsoring a contractor's report, or tasking agency, are entered in section 8.) DREP, FMO, Victoria, B.C. Canada VOS 1B0		2. SECURITY CLASSIFICATION (overall security classification of the document, including special warning terms if applicable) UNCLASSIFIED	
3. TITLE (the complete document title as indicated on the title page. Its classification should be indicated by the appropriate abbreviation (S,C or U) in parentheses after the title.) Modelling Arctic ambient noise in the 2 - 200 Hz band			
4. AUTHORS (Last name, first name, middle initial) Greening, Michael, V. and Zakarauskas, Pierre			
5. DATE OF PUBLICATION (month and year of publication of document) December 1993		6a. NO. OF PAGES (total containing information. Include Annexes, Appendices, etc.) 23	6b. NO. OF REFS (total cited in document) 21
7. DESCRIPTIVE NOTES (the category of the document, e.g. technical report, technical note or memorandum. If appropriate, enter the type of report, e.g. interim, progress, summary, annual or final. Give the inclusive dates when a specific reporting period is covered.) Technical Memorandum			
8. SPONSORING ACTIVITY (the name of the department project office or laboratory sponsoring the research and development. Include the address.)			
9a. PROJECT OR GRANT NO. (if appropriate, the applicable research and development project or grant number under which the document was written. Please specify whether project or grant)		9b. CONTRACT NO. (if appropriate, the applicable number under which the document was written)	
10a. ORIGINATOR'S DOCUMENT NUMBER (the official document number by which the document is identified by the originating activity. This number must be unique to this document.) DREP TM 93-79		10b. OTHER DOCUMENT NOS. (Any other numbers which may be assigned this document either by the originator or by the sponsor)	
11. DOCUMENT AVAILABILITY (any limitations on further dissemination of the document, other than those imposed by security classification) (X) Unlimited distribution () Distribution limited to defence departments and defence contractors; further distribution only as approved () Distribution limited to defence departments and Canadian defence contractors; further distribution only as approved () Distribution limited to government departments and agencies; further distribution only as approved () Distribution limited to defence departments; further distribution only as approved () Other (please specify):			
12. DOCUMENT ANNOUNCEMENT (any limitation to the bibliographic announcement of this document. This will normally correspond to the Document Availability (11). However, where further distribution (beyond the audience specified in 11) is possible, a wider announcement: audience may be selected.) UNLIMITED			

13. ABSTRACT (a brief and factual summary of the document. It may also appear elsewhere in the body of the document itself. It is highly desirable that the abstract of classified documents be unclassified. Each paragraph of the abstract shall begin with an indication of the security classification of the information in the paragraph (unless the document itself is unclassified) represented as (S), (C), or (U). It is not necessary to include here abstracts in both official languages unless the text is bilingual).

Short-term Arctic ambient noise spectra over the frequency band 2-200 Hz are presented along with a two-component noise model capable of reproducing these spectra. The model is based on the measured source spectrum and the spatial, temporal and source level distributions of both active pressure ridging and ice cracking. Modelled ambient noise levels are determined by summing the input energy of the distributions of ice cracking and pressure ridging events and correcting for the propagation loss. Both modelled and measured spectra show that ice cracking may dominate the spring-time ambient noise to frequencies as low as 40 Hz.

14. KEYWORDS, DESCRIPTORS or IDENTIFIERS (technically meaningful terms or short phrases that characterize a document and could be helpful in cataloguing the document. They should be selected so that no security classification is required. Identifiers, such as equipment model designation, trade name, military project code name, geographic location may also be included. If possible keywords should be selected from a published thesaurus, e.g. Thesaurus of Engineering and Scientific Terms (TEST) and that thesaurus-identified. If it is not possible to select indexing terms which are Unclassified, the classification of each should be indicated as with the title.)

AMBIENT NOISE

ARCTIC OCEAN

UNDERWATER ACOUSTICS

ICE RIDGES

ICE CRACKING

139297

NO. OF COPIES NOMBRE DE COPIES	COPY NO. COPIE N°	INFORMATION SCIENTIST'S INITIALS INITIALES DE L'AGENT D'INFORMATION SCIENTIFIQUE
1	1	DAR
AQUISITION ROUTE FOURNI PAR	▶	DRCP
DATE	▶	25 Feb 94
DSIS ACCESSION NO. NUMÉRO DSIS	▶	94-01288

DND 1158 (6-87)



**PLEASE RETURN THIS DOCUMENT
TO THE FOLLOWING ADDRESS:**

DIRECTOR
SCIENTIFIC INFORMATION SERVICES
NATIONAL DEFENCE
HEADQUARTERS
OTTAWA, ONT. - CANADA K1A 0K2

**PRIÈRE DE RETOURNER CE DOCUMENT
À L'ADRESSE SUIVANTE:**

DIRECTEUR
SERVICES D'INFORMATION SCIENTIFIQUES
QUARTIER GÉNÉRAL
DE LA DÉFENSE NATIONALE
OTTAWA, ONT. - CANADA K1A 0K2